

Evolution of Class 0 protostars: Models vs. Observations

D. Froebrich^{1*}, S. Schmeja², M.D. Smith^{3,4} and R.S. Klessen²

¹*Dublin Institute for Advanced Studies, 5 Merrion Square, Dublin 2, Ireland*

²*Astrophysikalisches Institut Potsdam, An der Sternwarte 16, D-14482 Potsdam, Germany*

³*Armagh Observatory, College Hill, Armagh BT61 9DG, Northern Ireland*

⁴*Centre for Astrophysics & Planetary Science, The University of Kent, Canterbury CT2 7NR, UK*

Received sooner; accepted later

ABSTRACT

The rates at which mass accumulates into protostellar cores can now be predicted in numerical simulations. Our purpose here is to develop methods to compare the statistical properties of the predicted protostars with the observable parameters. This requires (1) an evolutionary scheme to convert numerically-derived mass accretion rates into evolutionary tracks and (2) a technique to compare the tracks to the observed statistics of protostars. Here, we use a 3D-Kolmogorov-Smirnov test to quantitatively compare model evolutionary tracks and observations of Class 0 protostars.

We find that the wide range of accretion functions and timescales associated with gravito-turbulent simulations naturally overcome difficulties associated with schemes that use a fixed accretion pattern. This implies that the location of a protostar on an evolutionary track does not precisely determine the present age or final accrued mass. Rather, we find that predictions of the final mass for protostars from observed $T_{\text{bol}}\text{-}L_{\text{bol}}$ values are uncertain by a factor of two and that the bolometric temperature is not always a reliable measure of the evolutionary stage. Furthermore, we constrain several parameters of the evolutionary scheme and estimate a lifetime of Class 0 sources of $2\text{-}6 \cdot 10^4$ yrs, which is related to the local free-fall time and thus to the local density at the onset of the collapse. Models with Mach numbers smaller than six are found to best explain the observational data. Generally, only a probability of 70 % was found that our models explain the current observations. This is caused by not well understood selection effects in the observational sample and the simplified assumptions in the models.

Key words: Accretion, accretion discs - Methods: numerical - Methods: statistical - Stars: formation - Stars: statistics

1 INTRODUCTION

A major challenge still remaining in astronomy is to determine how mass accumulates to form stars. We now know from observations that almost the entire mass of a star like the Sun is gained during a short protostellar stage (Adams et al. (1987)). Some of these protostellar objects are luminous yet cool, suggesting the existence of an even briefer phase within which the protostar accretes rapidly from a highly obscuring core (André et al. (1993)). The existence of this so-called Class 0 phase, however, highlights the need for the development of models which predict how a protostar abruptly evolves. A successful model would also predict the total accumulated mass or ‘final mass’, providing a fundamental input for the subsequent stellar evolution. However, it is debatable whether the development of low mass stars can be described by an evolutionary model or if the systems are simply too complex and diverse.

To further the debate, we require three factors: reliable obser-

vations of protostars, models for how cores form and collapse out of a molecular cloud and a means of converting model parameters into observational parameters. Here, we develop a statistical method for comparing observational data to model data and proceed to test the method by making a specific comparison. This requires us to develop an appropriate technique to compare data within a three dimensional parameter space. We first introduce, in turn, the data, the model and the interfacing scheme.

The protostellar stage begins soon after the start of collapse of the cloud core. Half of the final stellar mass is gained in the very earliest, deeply embedded phase. Further accretion occurs during the Class 1 phase while an accretion disk still feeds material in the extended Class 2 stage. The number of observable Class 0 sources at any given instant is relatively small, due to their brief lifespans. In addition they are difficult to detect since their massive envelopes cause their spectral energy distributions (SED) to peak in the far infrared. Consequently, a variety of strategies have been adopted to discover Class 0 sources: (1) Large scale imaging for outflows in the optical or near infrared (NIR; e.g. Ziener

* E-mail: df@cp.dias.ie

& Eislöffel (1999); Stanke et al. (2002)); (2) High resolution processing of IRAS data (e.g. Hurt & Barsony (1996); O’Linger et al. (1999)); (3) sub-millimetre or millimetre continuum mapping (e.g. Shirley et al. (2000); Motte & André (2001)); (4) deep radio continuum or line surveys (e.g. Bontemps et al. (1995); Bourke et al. (1997)). Therefore it is evident to keep in mind that source samples are subject to strong selection effects.

We require a statistically significant observational sample of protostars with accurate individual properties. The latter demand a uniform observational coverage of the entire SED from the NIR to the millimetre range. Froebrich (2005) recently presented a catalogue with all known confirmed and candidate Class 0 sources in the literature. This catalogue contains 50 objects that possess sufficient observational data to compute the three main source properties (bolometric temperature and luminosity, envelope mass; T_{bol} , L_{bol} , M_{env}) accurately.

We can potentially test a range of cloud models. Each model assumes a particular environment, with initial conditions, boundary conditions, external forces and feedback effects to be considered (Mac Low & Klessen (2004)). However, in the present study, our attention is focused on a set of accretion rates obtained from numerical simulations of turbulent clouds (see § 2.2; Schmeja & Klessen (2004); hereafter SK04). The mass distribution of the cores so formed can be compared to the initial mass function and the total mass fraction accumulated in protostellar cores can be related to the overall star-formation efficiency (Klessen (2001b), Padoan & Nordlund (2002)). These recent numerical studies are able to provide an almost complete model of star formation in clusters, including the formation of disks and binary systems (see also Bate et al. (2003)). As a more fundamental test of these models, we need to compare model predictions to the observable properties of stars caught in the act of forming (T_{bol} , L_{bol} , M_{env}). The numerical models used here, as well as the works from other groups (e.g. Bate et al. (2003)) are only able to follow the density and velocity of material. They are hence very useful in obtaining final mass spectra, binary fraction, etc.. However, they are not able to predict observables like bolometric temperature and/or luminosity. To derive those quantities, in principle a 3D radiative transfer calculation needs to be performed at each time step. Since this is much too time consuming we applied an evolutionary scheme to obtain those quantities (see Sect. 2.3).

Alternatively, mass accretion rates can be calculated from theoretical and semi-empirical approaches. In the so-called “standard solution” of the collapse of an isothermal sphere (Shu (1977)) the mass accretion rate is constant at a value of $0.975 c_s^3 / G$, where c_s is the sound speed and G the gravitational constant. Larger but also constant accretion rates ($47 c_s^3 / G$) are found by Larson (1969) and Penston (1969) for the collapse of initially uniform isothermal spheres. Henriksen et al. (1997) find that mass ejection and mass accretion both decline significantly with time during protostellar evolution. Using a Plummer-type density profile Whitworth & Ward-Thompson (2001) predict an accretion rate that possesses a very early peak during the Class 0 phase and falls off rapidly after the object develops into a Class 1 protostar. Shu et al. (2004) obtained similar results through analytical and numerical works. Hydrodynamical simulations of star formation (Foster & Chevalier (1993); Tomisaka (1996)) controlled by supersonic turbulence (e.g. Klessen (2001a); SK04) yield similar behaviour.

In theory, there are two means to interface model and observed data sets. Ideal would be to derive a set of mass accretion rates directly from observations of protostellar cores but infall speeds are extremely difficult to measure. Hence, conversely, we convert the mass infall rates from the models into the observable quantities.

The main three are the bolometric temperature and luminosity, T_{bol} and L_{bol} , and the envelope mass, M_{env} .

Several such conversion schemes have been developed. Evolutionary models were first discussed by Bontemps et al. (1996) and Saraceno et al. (1996). Along these lines, André et al. (2000) took an exponentially decline in both envelope mass and accretion rate to predict $L_{\text{bol}}-M_{\text{env}}$ tracks. An analytical scheme was presented by Myers et al. (1998). They assumed a mass infall rate matching the Shu solution at early times and then displaying an exponential fall off with time. The core which supplies the mass also provides the obscuration, thus fixing evolutionary tracks on a $T_{\text{bol}}-L_{\text{bol}}$ diagram. Based on this work, Smith ((1998; 2000; 2002); S98 hereafter) presented an evolutionary scheme but adopted alternative analytical forms for the mass accretion (exponential increase and power law decrease) which resemble the results obtained by Whitworth & Ward-Thompson (2001) or SK04. This evolutionary model, founded on mass transfer between the envelope, disc, protostar and jets, has provided successful interpretations for various sets of observational data (T_{bol} , L_{bol} , M_{env} , outflow luminosity) of Class 0 and Class 1 objects (e.g. Davis et al. (1998); Yu et al. (2000); Stanke (2000); Froebrich et al. (2003)). Here, we adopt the S98 scheme but replace the analytical accretion rates with those derived numerically. We note that this scheme does not include any inclination effects that become very important during the Class 1 phase for T_{bol} and L_{bol} determinations. We thus focus our work on Class 0 objects.

Our approach in this paper is as follows. We combine different sets of mass accretion rates obtained from gravoturbulent molecular cloud fragmentation calculations (gt-models; Klessen et al. (2000); Klessen (2001a); Appendix A), as described in detail in SK04, and the evolutionary scheme (e-model) from S98 (see also Appendix B). For each set of mass accretion rates, we determine evolutionary tracks in the $T_{\text{bol}}-L_{\text{bol}}-M_{\text{env}}$ parameter space and compare them with the distribution of the observed Class 0 sample. A 3D-Kolmogorov-Smirnov test (KS-test, see also Appendix C) yields a probability for the two distributions to be drawn from the same basic population (called *agreement* hereafter). The agreement parameter will thus determine how well a model is able to explain the currently available set of observations.

We remark that two separate models (gt-models and e-models) are needed to obtain the model protostellar quantities that can be compared to the observational data. Thus, we are only able to determine how well the *combination* of *both* can explain the observations. We are not able to decide which model is responsible for potential disagreement with the observations. However, the variation of free parameters in the models and a search for correlations of the parameter values with the agreement will help to define constraints and provide suggestions for improved model combinations.

In Sect. 2 we describe the observational data and our models. Results and the discussion are put forward in Sect. 3. Details of the gravoturbulent and evolutionary models and the Kolmogorov-Smirnov test are described in Appendixes A to C.

2 OBSERVATIONS AND MODELS

2.1 Observational data

Several samples of Class 0 sources have been published (e.g. Chen et al. (1995); André et al. (2000); Shirley et al. (2000); Motte & André (2001)). The latest study, which combines all previous ones and computes the object properties uniformly from all published

data, is presented by Froebrich (2005). There, a list of 95 confirmed or candidate objects was compiled. Fifty of these sources possess sufficient observational data to be classified as Class 0 or Class 0/1 objects and allow us to determine the three source properties T_{bol} , L_{bol} , and M_{env} accurately. To ensure a reliable comparison of models and observations, we apply the following restrictions to this sample:

(1) We omit sources that have distances larger than 500 pc. This reduces the bias towards higher mass objects.

(2) All objects in Taurus are underluminous compared to the other sources, considering T_{bol} and M_{env} . Note that this does not only mean a low luminosity for these objects, but rather a low luminosity combined with a high envelope mass. The three very low luminosity objects in our sample (see Fig. 1) combine low luminosity ($1 L_{\odot}$) with low envelope mass ($0.2 M_{\odot}$) and might form (very) low mass stars. In total, 25 % of the Class 0 objects in the sample are underluminous. We exclude them for the comparison between the models and observations (but see the discussion in Sect. 3.6).

(3) A histogram of the number of sources in a certain T_{bol} -bin shows that the observational sample is very incomplete at high bolometric temperatures. Hence the comparison of observations and models is restricted to $T_{\text{bol}} < 80$ K.

This selection procedure leaves us with a sample of 27 Class 0 sources. This sample consists mostly of objects in Perseus, Orion and Serpens.

2.2 Gravoturbulent models

We performed numerical simulations of the fragmentation and collapse of turbulent, self-gravitating gas clouds and the resulting formation and evolution of protostars. We employed a code based on smoothed particle hydrodynamics (SPH; Monaghan (1992)) in order to resolve large density contrasts and to follow the evolution over a long timescale. The code includes periodic boundary conditions (Klessen (1997)) and sink particles (Bate et al. (1995)) that replace high-density cores while keeping track of mass, linear and angular momentum. A detailed study of the 24 sets of protostellar mass accretion rates resulting from the gt-models is presented in SK04 (see also Jappsen & Klessen (2004)) and we adopt their gt-model notation.

We now define when a model core is considered to be a Class 0 object. Observationally, a protostar is a Class 0 source according to the definition given in André et al. (2000). It is shown by André et al. (1993) that this definition is roughly equivalent to the physical state where the mass in the envelope exceeds the mass of the central protostar. Thus, a model protostar is considered a Class 0 object when (a) the mass of the central core exceeds $10^{-2} M_{\odot}$ (this corresponds to the time when the second hydrostatic core is formed in the centre (Larson (2003)) and distinguishes the Class 0 sources from the pre-stellar core phase) and (b) the mass of the envelope is larger than the mass of the central star. This separates the Class 0 from the Class 1 objects.

Small number statistics will always be a major concern when comparing models and observations of Class 0 objects. In order not to introduce further uncertainties from the model side, we restricted our analysis to those gt-models that possess more than 37 stars and have a numerical resolution of at least $2 \cdot 10^5$ particles. This leaves 16 out of the 24 sets of accretion rates of SK04 for further analysis. In addition, accretion rates for individual protostars from the gt-models are smoothed by a viscous time scale of the accretion disc of $\sim 10^4$ yrs (see Appendix A for details).

A small fraction of model protostars were highly accelerated

Table 1. Variable parameters from the e-model of S98, together with the range they were varied in and the original value. The last two columns provide the overall range found to lead to the best agreement.

Parameter	varied		org. value	best	
	from	to		from	to
T_{env} [K]	10	30	24	15	19
$frac_{\text{env}}$ [%]	75	100	87	86	96
M_{extra}	0	5	2	1.0	2.4
t_0 [10^3 yrs]	1	100	30	30	80
α	0.5	4.0	1.75	1.4	3.2
R_{in} [AU]	5	100	30	35	80
M_{eff} [%]	0	50	30	36	44
p	1.4	2.0	1.5	1.55	1.80
κ [$\text{cm}^2 \text{g}^{-1}$]	2	6	4	3.0	5.0

(e.g. by ejection from a multiple system). Due to the adopted periodic boundary conditions in our calculations, these objects cross the computational domain many times while continuing to accrete. In reality, however, these protostars would have quickly left the high-density gas of the star-forming region and would not be able to gain more mass. We therefore consider accretion to stop after the object has crossed the computational box more than ten times.

The radius of a sink particle is fixed at 280 AU, the physics (e.g. exact accretion, radiation) inside this volume cannot be resolved. Therefore, an evolutionary model describing the processes inside the sink particle is required.

2.3 Evolutionary scheme

The e-model is used to transform the mass accretion rates from the gt-models into observable quantities such as T_{bol} , L_{bol} , and M_{env} . It is based on mass and energy transfer between the different components of the forming star (protostar, disc, envelope, jet). Mass conservation is the main principle in this analytical model. Each simulated accretion rate from the gt-models is taken as the mass inflow rate from a spherical envelope onto the inner disc/protostar/jet system. All the mass flows through the disc but only a fraction accretes onto the protostar. The rest is ejected within two jets. The ejected mass fraction is small but not negligible in the Class 0 stage. See Appendix B for a detailed description of the parameters and equations of the evolutionary model used in this work.

Many parameters and constants are needed to fully describe the envelope and predict the radiative properties (Myers et al. (1998), S98, Appendix B). We carefully chose a subset of parameters which we kept variable: (1) T_{env} ; The temperature of the outer envelope, out to which the envelope mass is determined. (2) $frac_{\text{env}}$; The total mass that will be accreted onto the protostar is distributed in the envelope and the disc. A constant ratio of these two masses is assumed and $frac_{\text{env}}$ represents the fraction of the total mass that is in the envelope. (3) M_{extra} ; This is the supplementary mass fraction in the immediate surroundings which does not actually fall towards the star, to be accreted or jetted away, but is removed directly from the core probably through a feedback process. See Eq. B7 for the exact definition used. (4/5) t_0 , α ; These two parameters describe the dispersion of the extra mass in the envelope. (6) R_{in} ; The inner radius of the envelope. (7) M_{eff} ; The maximum percentage of the infalling envelope mass which is ejected into the outflow. (8) p ; The power-law index of the density distribution in the envelope, assumed constant in time. (9) κ ; The opacity of the

envelope material at $12\ \mu\text{m}$. In Table 1 we list the parameter ranges which were tested.

We now only need to impose a mass accretion rate from the gt-models for the evolution of a model protostar to be fully determined. Using all individual accretion rates in a gt-model allows us to build up a $T_{\text{bol}}\text{-}L_{\text{bol}}\text{-}M_{\text{env}}$ distribution which can be compared to the observational dataset.

Some of our free parameters can be, and have been, observed for individual objects. This includes for example the power-law index of the density distribution in the envelope (e.g. Chandler & Richer (2000), Motte & André (2001)) or $frac_{\text{env}}$ (e.g. Looney et al. (2003)). We chose to keep those parameters variable in order to test our method, since we expected to obtain values within the observational constraints.

2.4 3D KS-Test and probabilities

The best way to compare two distributions of data points is through a Kolmogorov-Smirnov test. This test yields the probability of two distributions being drawn from the same basic population. In one dimension, the KS-test compares the cumulative probability functions of a sample and a model and for large sample sizes the probability can be determined analytically. Since our distributions are three dimensional ($T_{\text{bol}}\text{-}L_{\text{bol}}\text{-}M_{\text{env}}$), there are no analytical means to perform such a test. We therefore generalised the method of a two dimensional KS-test (e.g. Singh et al. (2004)) for our purpose. The basic result of this test is the value $D_{3\text{D}}$ that ranges from zero to one. The lower this value the better the two distributions match. Using a Monte Carlo method $D_{3\text{D}}$ can be converted to the agreement ($P_{3\text{D}}$), which gives the probability that the two distributions are drawn from the same population.

The task of finding the parameter set for the e-models that results in the highest agreement is a multi-dimensional, non-linear, minimisation problem. We solved this using a Monte Carlo approach. In Appendix C we outline the details of this method which allows to constrain the range for the e-model parameters and to determine the best agreement.

3 ANALYSIS & DISCUSSION

3.1 Evolutionary tracks

One of our goals is to investigate the accuracy to which the final mass of a protostar (M_{final}) can be estimated from its present location in the $T_{\text{bol}}\text{-}L_{\text{bol}}$ diagram. To achieve this, we sort for each gt-model the individual model stars into final mass bins with a width of 0.3 in logarithmic units (equivalent to a factor two in mass). The following ranges for the mass bins were chosen: <0.2 , $0.2\text{...}0.4$, $0.4\text{...}0.8$, $0.8\text{...}1.6$, $1.6\text{...}3.2$, $\geq 3.2 M_{\odot}$. The particular size of the mass bins was adopted in order to ensure a reasonably large number of stars in each bin for the gt-models. Depending on the mass function and the total number of objects in the gt-model, there are up to 20 objects per bin for the lower masses ($M_{\text{final}} \leq 1.6 M_{\odot}$). The higher mass bins naturally suffer from a paucity of objects.

We determined for every gt-model the average accretion rate history in each mass bin. These mean accretion rates are then used to determine evolutionary tracks in the $T_{\text{bol}}\text{-}L_{\text{bol}}$ diagram. The left column of Fig. 1 shows the tracks for the six mass bins of the models M05k8, M2k2, and M6k2a as an example. The lowest final masses correspond to the thinnest line, and so forth. Note that the average evolutionary tracks show higher L_{bol} at a given T_{bol}

for higher final star masses. This represents the fact that stars with higher final masses on average have higher accretion rates (SK04) and hence bolometric luminosities.

Further we analysed the individual evolutionary tracks. As an example, we plot all individual tracks for the same three models with final stellar masses in the range 0.8 to $1.6 M_{\odot}$ (mass bin 4, solar mass stars) in the middle column of Fig. 1. These tracks are determined assuming typical e-model parameters from the range that best fit the observations (see below). We find that all tracks show a similar general behaviour. The tracks start off at $T_{\text{bol}} \approx 15$ K for solar mass stars. Lower mass Class 0 sources start off at higher temperatures. Then they show a gradual increase in luminosity until the end of the Class 0 phase. Some notable exceptions are evident in Fig. 1, which imply that T_{bol} is not always a reliable guide as to the envelope-protostar mass ratio.

Are we able to estimate the final mass of a Class 0 source from its position in the $T_{\text{bol}}\text{-}L_{\text{bol}}$ diagram? To address this question, we determined the $1\ \sigma$ scatter of the individual tracks at each time step in all mass bins. In the right column of Fig. 1 this scatter is shown for mass bin 4 as thin lines. Almost independent of the gt-model, we find that the scatter has about the size of the separation between tracks for two adjacent mass bins. Hence, we conclude that from a certain position in the $T_{\text{bol}}\text{-}L_{\text{bol}}$ diagram, *we are only able to estimate the final mass of the protostar to within a factor of two*. Note that this estimate does not take into account possible errors in the measurement of T_{bol} and L_{bol} , as well as possible different accretion histories. This supports the notion that other observables might be more adequate for dating Class 0 protostars, e.g. the $L_{\text{smm}}/L_{\text{bol}}$ ratio (Young & Evans (2005)), in agreement with the original observational definition of Class 0 sources (André et al. (1993)).

We further find that tracks determined from averaged accretion rates noticeably differ from the averaged evolutionary tracks of the individual stars. This is evident in the right column of Fig. 1 which shows as a thick line the track from the averaged accretion rate. At some points, it approaches or even lies outside the $\pm 1\ \sigma$ range of the individual evolutionary tracks. This clearly shows, together with the findings in the above paragraph, that the individual accretion history significantly influences the position in the $T_{\text{bol}}\text{-}L_{\text{bol}}$ diagram, in addition to the final stellar mass.

The general behaviour of the $T_{\text{bol}}\text{-}L_{\text{bol}}$ tracks (characteristics of the individual tracks, the average tracks, and the scatter around the average) is independent of the considered mass bin and gt-model.

3.2 Distribution in $T_{\text{bol}}\text{-}L_{\text{bol}}\text{-}M_{\text{env}}$

In Fig. 2 we show how the model tracks (M05k8, M2k2, M6k2a, from left to right) are distributed in the full $T_{\text{bol}}\text{-}L_{\text{bol}}\text{-}M_{\text{env}}$ parameter space. The grey-scale background of the individual panels gives the probability to find one of the model stars at this particular position. Darker regions indicate higher probabilities. We used typical e-model parameters (see Table 2) to determine these diagrams. For comparison the observational datapoints are overplotted. Note that we plotted only model points with $T_{\text{bol}} < 80$ K, as this is the limit of the observational data and only these are used in the comparison with the observations.

As evident in Fig. 2, the model distributions cover roughly the same area as the observations. Especially in the $T_{\text{bol}}\text{-}L_{\text{bol}}$ and $T_{\text{bol}}\text{-}M_{\text{env}}$ plane the models are able to explain the peak in the observed distribution. In the $L_{\text{bol}}\text{-}M_{\text{env}}$ plane, however, the models fail to explain this peak (see right column in Fig. 2). Our models predict smaller envelope masses (by a factor of two) compared to parts

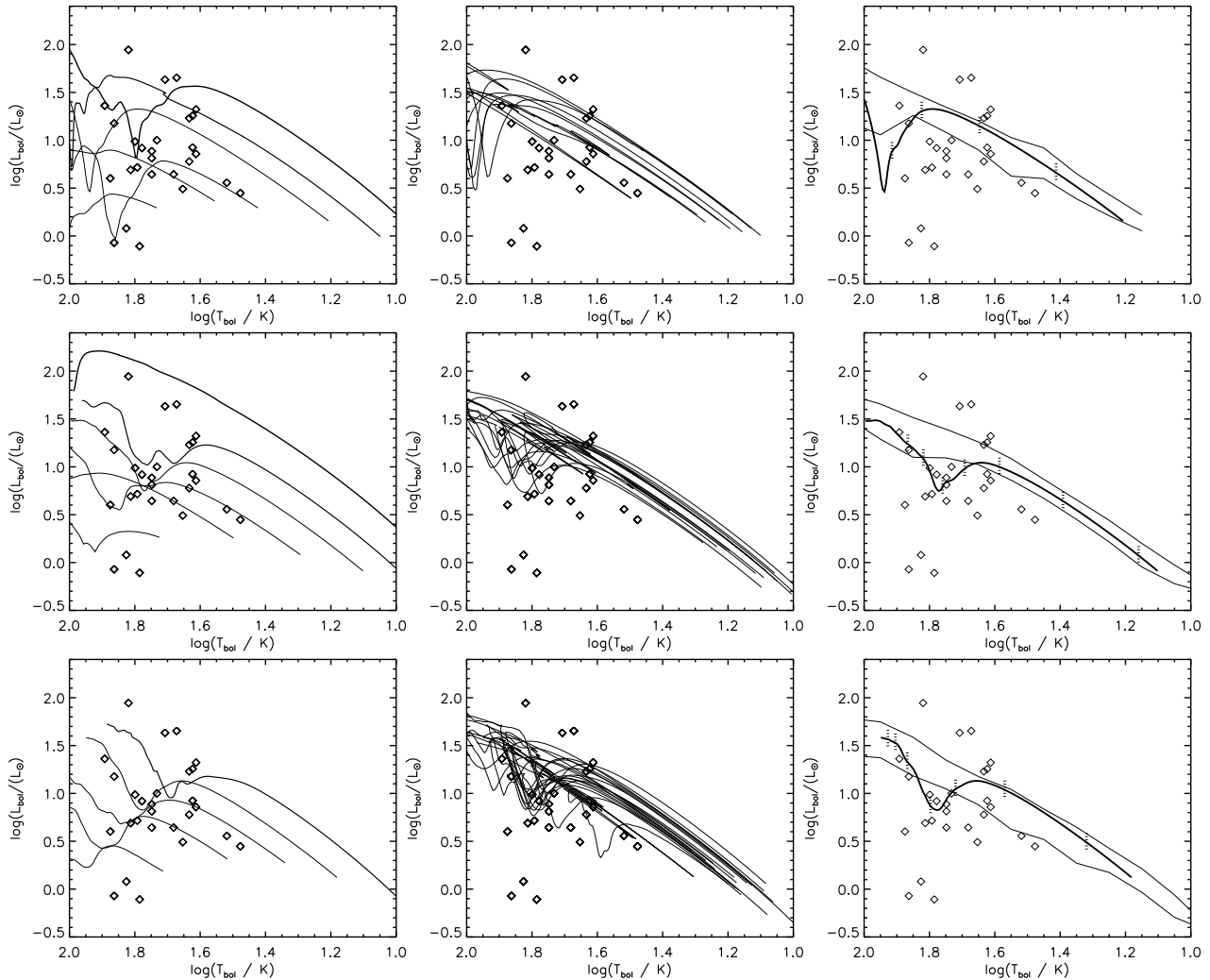


Figure 1. Evolutionary tracks in the $T_{\text{bol}}-L_{\text{bol}}$ parameter space of the model Class 0 sources in the gt-models M05k8 (top row), M2k2 (middle row), and M6k2a (bottom row). The tracks are determined using typical e-model parameters from the range best fitting the observations (see Table 2). Left column: Tracks for the average accretion rates in the six mass bins. Thicker lines correspond to higher final masses. Note that there are no stars in mass bin 6 in the M6k2a model. Middle column: All individual tracks in mass bin 4. Right column: Track for average accretion rate of stars in mass bin 4 (solar mass stars; thick line) and the $\pm 1\sigma$ scatter of the individual tracks (thin lines). The vertical lines mark ages of the sources starting from $5 \cdot 10^3$ yrs in steps of $5 \cdot 10^3$ yrs. The open diamonds in each panel mark the positions of the observational sample (taken from Froebrich 2005). See Sect. 3.1 for more details.

of the observations. Considering the cluster of observational points at about $M_{\text{env}} = 1 M_{\odot}$, the discrepancy could be a selection effect in the observations. In addition, observed envelope masses are uncertain by a factor of two (Motte & André (2001)). See also the discussion in Sec. 3.7.

3.3 Initial mass function

We analyse the mass function of the final masses of model stars (IMF) in the gt-models in order to compare it to that of the observational sample. The protostellar mass functions of the gt-models show a decline for masses larger than about $0.3 M_{\odot}$. The mean value of the slope of all considered models is $\langle \Gamma \rangle = -0.84$ in the mass range $-0.5 < \log M/M_{\odot} < 1$. This is less steep than the Salpeter slope of -1.35 (Salpeter (1955)) but our results are biased by the fact that binaries or multiple systems cannot be resolved. At the low-mass end, the mass function is constrained by the SPH resolution limit of $\sim 0.05 M_{\odot}$. Nevertheless, the mean value is in good

agreement with the estimated final stellar mass spectrum in the corresponding observational sample ($\Gamma = -0.9 \pm 0.2$; Froebrich (2005)). Recall, that for this sample also no binary correction has been made.

We test if the slope of the IMF in the gt-models is related to the best agreement (P_{3D}). However, no systematic dependence of P_{3D} on Γ is present. In particular, a good agreement of Γ between the gt-model and the observations does not necessarily lead to a high P_{3D} -value. As discussed in the last paragraph (see also the middle panel of Fig. 1), the differences in the position in the $T_{\text{bol}}-L_{\text{bol}}$ diagram are partly due to the accretion history and not due to the final mass. Hence, the test performed here is much more sensitive to the distribution of individual accretion histories than to the slope of the IMF.

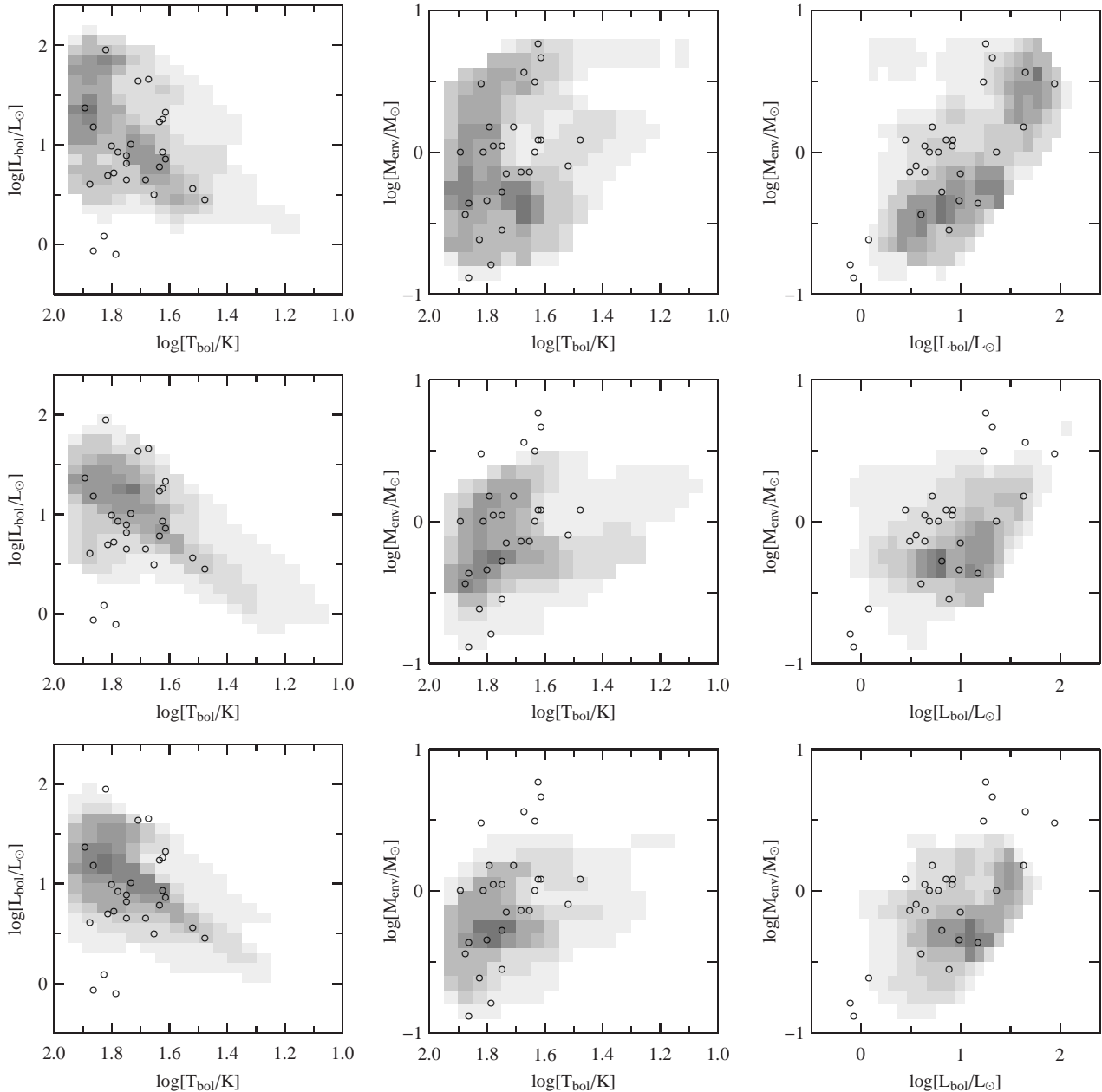


Figure 2. Distribution of Class 0 observations (circles) and models (grey-scale) in the $T_{\text{bol}}\text{-}L_{\text{bol}}$ (left column), $T_{\text{bol}}\text{-}M_{\text{env}}$ (middle column), and $L_{\text{bol}}\text{-}M_{\text{env}}$ (right column) plane of the parameter space. The plots are shown for the models M05k8 (top row), M2k2 (middle row), and M6k2a (bottom row). Darker grey-values in the model distribution corresponds to higher density of model points. As in Fig. 1 typical e-model parameters are used for the model distributions (see Table 2). Only model points with T_{bol} smaller than 80 K are shown in the plots since this is the limit of the observational data.

3.4 Evolutionary model

To constrain the free parameters in the e-model, we investigate here how the chosen values influence the agreement P_{3D} . Table 2 contains the range of values which provide the highest agreement for each gt-model. In particular we show the values for the best fitting 5% of the e-models. It is more meaningful to provide these ranges instead of the particular parameters for the single best fitting model. These are statistically less significant, since not the whole parameter space is tested by our method. We obtain the following results for all gt-models:

- The temperature at the outer envelope boundary is lower than

the standard value of 24 K. Typically temperatures between 15 and 19 K lead to a good agreement.

- A wide range for inner envelope radii (R_{in}) leads to high P_{3D} . Values from 35 to 80 AU are typical. This wide range is in agreement with the fact that a change in R_{in} , while fixing all other parameters, usually results in very small changes of P_{3D} . However, the range for the best fitting models does not include the hitherto standard value of 30 AU.

- In most cases small amounts of extra mass in the envelope ($1.0 < M_{\text{extra}} < 2.4$) lead to high agreement.

- The parameter α shows a wide range of possible values for a good agreement ($1.4 < \alpha < 3.2$). A similar wide range is found for

Table 2. Parameter ranges needed in the e-model to best match the observational data (see Appendix B for details on the parameters). We list the values for the best fitting 5 % of the parameter combinations. The last two columns list the median and average duration of the Class 0 phase of the individual stars in the models.

Model	T_{env} [K]	$frac_{env}$ [%]	M_{extra}	t_0 [10^3 yrs]	α	R_{in} [AU]	M_{eff} [%]	p	κ [$cm^2 g^{-1}$]	D_{3D}	P_{3D} [%]	t_{CI0}^{med} [10^3 yrs]	t_{CI0}^{ave} [10^3 yrs]
G2	15-19	81-89	0.6-2.4	35-75	1.4-3.2	30-80	44-47	1.6-1.9	3.0-5.2	0.30-0.37	37.2 - 5.93	41	44
M01k2	14-18	87-95	1.0-2.8	20-85	1.4-3.4	40-75	28-44	1.6-1.8	3.0-4.6	0.37-0.41	12.2 - 2.43	39	41
M05k4	17-20	89-94	1.2-2.0	35-75	1.6-3.2	45-85	41-44	1.5-1.7	3.0-4.4	0.29-0.37	40.3 - 4.72	31	36
M05k8	16-19	90-95	0.9-2.0	25-80	1.9-3.0	40-85	40-46	1.5-1.7	3.0-4.6	0.36-0.43	45.9 - 6.53	31	34
M2k2	15-20	86-92	1.0-2.4	35-85	1.6-3.2	35-80	35-43	1.5-1.7	3.4-5.2	0.29-0.36	73.1 - 19.6	32	39
M2k4	15-18	86-92	1.0-2.4	35-75	1.4-3.2	40-75	39-43	1.5-1.7	3.2-5.2	0.48-0.52	30.5 - 4.69	15	23
M2k8	13-18	80-90	1.0-2.2	30-75	1.2-3.6	35-75	32-41	1.5-1.7	3.4-5.4	0.27-0.34	67.4 - 17.0	45	56
M3k2	15-18	82-94	0.6-2.6	20-90	1.4-3.6	35-85	37-44	1.5-1.8	2.8-4.6	0.28-0.35	55.1 - 10.8	44	43
M3k4	12-14	80-92	0.6-1.6	25-80	1.4-3.4	30-70	32-44	1.5-1.8	3.2-5.2	0.33-0.40	5.99 - 0.53	87	105
M6k2a	16-20	85-95	1.0-2.4	20-85	1.4-3.4	45-85	35-43	1.6-1.8	2.8-4.6	0.32-0.36	46.5 - 20.4	26	32
M6k4a	15-20	93-97	0.8-3.2	40-80	1.4-3.2	30-70	12-34	1.6-1.8	3.2-5.2	0.47-0.50	0.05 - 0.01	38	120
M6k2b	15-20	82-94	1.2-3.0	35-80	1.6-3.2	35-75	36-40	1.6-1.8	3.2-5.4	0.35-0.40	14.2 - 2.84	26	35
M6k2c	15-20	86-96	1.0-3.0	35-75	1.4-3.2	35-75	36-42	1.6-1.9	3.4-4.8	0.38-0.43	5.30 - 0.62	29	51
M6k4c	13-18	82-85	0.6-2.6	20-85	1.2-3.2	30-80	28-44	1.5-1.8	3.0-5.2	0.45-0.51	22.2 - 2.57	14	54
M10k2	16-22	92-96	1.0-3.6	25-70	1.2-3.0	35-80	10-42	1.6-1.9	3.2-5.4	0.60-0.62	0.003 - 0.00	19	24
M10k8	14-17	93-98	0.8-3.2	30-85	0.8-3.8	35-80	16-38	1.5-1.7	3.4-5.2	0.43-0.49	2.60 - 0.23	44	124

t_0 which ranges from 30 to $80 \cdot 10^3$ yrs. The larger values found for t_0 suggest that the additional mass stays longer in the envelope to sustain low bolometric temperatures.

- A range of values of p is found to be able to best explain the data. However, in the majority of the cases $1.55 < p < 1.80$ leads to the best results. These values are in between the theoretical solutions for a free falling envelope (1.5) and a singular isothermal sphere (2.0). The range found here seems to be a compromise between younger and older objects. Since there are probably more older sources in the sample, the best values are closer to $p = 1.5$. In principle an evolution from $p = 2.0$ to $p = 1.5$ would be expected. Our findings do not contradict this. Our obtained values are in good agreement with (sub)-mm observations of envelopes (Chandler & Richer (2000); Motte & André (2001)).

- We found the mass fraction in the envelope to be in the range from 86 to 96 %. This would imply a disc mass of 4 to 14 % of the envelope mass, mostly smaller than the standard value of 13 % used so far, but in agreement with millimetre interferometric observations (e.g. Looney et al. (2003)).

- The amount of mass ejected into the jets is found to range from 36 to 44 %. This is a narrow range and somewhat contradictory to the observations and jet launching models which predict that at maximum 30 % of the material is ejected into the jets. We interpret the high amount of ejected material here as a combination of two things. (1) Material really ejected into the jets. (2) Material accreted onto the star, but the resulting luminosity escapes directly through the cavity generated by the jets and is not observed. If the accretion luminosity is radiated uniformly away, then the additional ejected material would imply opening angles between 30 and 60 degrees for the cavities, not an untypical value for many of the older Class 0 sources (e.g. Padman et al. (1997)). To conclusively prove this hypothesis one needs to include the outflow luminosity for all objects into the comparison of models and observations.

- The best-fitting opacity range (3.0 to $5.0 \text{ cm}^2 \text{ g}^{-1}$) agrees very well with the standard value of $4 \text{ cm}^2 \text{ g}^{-1}$.

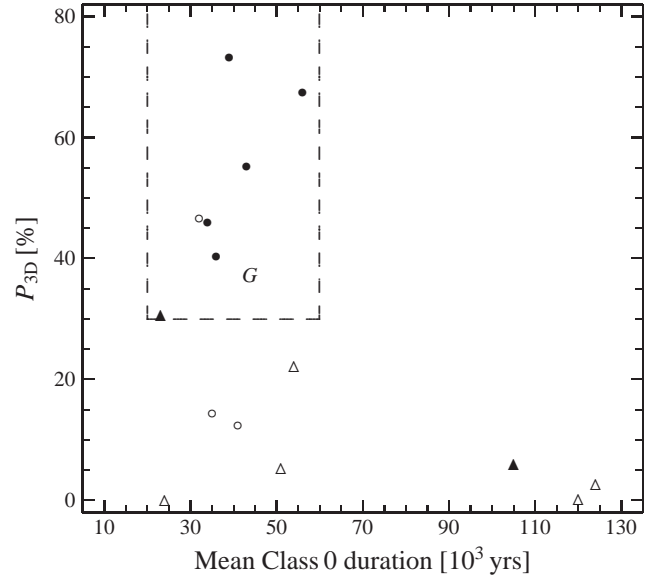


Figure 3. Mean duration of the Class 0 phase of the model stars vs. the P_{3D} value for the gravoturbulent models. Circles mark models that possess a median duration of the Class 0 phase between 2 and $6 \cdot 10^4$ yrs and a ratio of median to mean duration of the Class 0 phase of higher than 0.7 . Triangles mark models where one of these conditions is not fulfilled. Gravoturbulent models with Mach numbers in the range $0.5 \leq \mathcal{M} \leq 3.0$ are shown as filled symbols, models outside this range as open symbols. The Gaussian collapse model is marked as ‘G’. The dashed lines enclose the region where a high agreement of the models with the observations was found.

3.5 Gravoturbulent models

We now investigate if the initial conditions of the gt-models influence the agreement with the observations and the best fitting e-model parameters. The first point to note is that we find no significant correlations of any of the obtained parameter values of the e-models with the Mach number or wavelength that characterise the turbulence in the gt-model.

There are, however, large differences in the quality of agree-

ment between the various gt-models and the observations. In the following we investigate the cause of these differences. We determined for each set of accretion rates the median and the mean duration of the Class 0 phase of the model stars. The median for all gt-models ranges from 14 to $87 \cdot 10^3$ yrs, while the mean duration spans from 23 to $124 \cdot 10^3$ yrs. The much wider range for the average duration is due to some model stars (outliers) that go through an extremely long Class 0 phase. These objects have a large, secondary accretion peak which in many cases might not be physical but is caused by the lack of feedback mechanisms. Due to the mass criterion used, such peaks shift the transition from Class 0 to 1 to later times. In Table 2 we list the median and mean duration of the Class 0 phase of all stars in the models in the last two columns.

All gt-models with P_{3D} -values larger than 30 % are associated with a mean duration of the Class 0 phase between 2 and $6 \cdot 10^4$ yrs. Most of them possess a ratio of median to mean duration of the Class 0 phase exceeding 0.7. This indicates that no or only a few outliers are present in the set of accretion rates. When applying these two conditions to all gt-models, we select nine of them (circles + G in Fig. 3). Only M01k2 (12.2 %) and M6k2b (14.2 %) do not possess $P_{3D} > 30$ %. Hence 80 % of the gt-models with these properties lead to high agreement. There are seven models that do not fulfil one of the criteria (triangles in Fig. 3). Six of these possess P_{3D} -values smaller than 30 %. Hence 85 % of the gt-models that do not comply with both criteria lead to low agreement. This shows that high P_{3D} -values are only obtained for gt-models that generate few outliers and the ‘right’ duration of the Class 0 phase.

The duration of the Class 0 stage shows a linear correlation with the median of the fit parameter τ of SK04. This parameter indicates the time it takes until the peak accretion rate is reached. It is related to the local free-fall time and, thus, can be used as a rough estimate of the average density of the core at the onset of collapse (see SK04 for details). Given our best fitting models and the corresponding Class 0 lifetimes, we infer a range of $1.5 \cdot 10^5 \text{ cm}^{-3}$ for the local density at the start of the collapse. This is in good agreement with measured central densities of pre-stellar cores (e.g. Bacmann et al. (2002)). Our results thus suggest that stars in the observational sample may only form in pre-stellar cloud cores that reach a central density of order of 10^5 cm^{-3} . Obviously, the duration of the Class 0 phase depends directly on the initial local density.

As can be seen in Table 2, gt-models with Mach numbers $0.5 \leq M \leq 3$ best describe the observations (filled symbols in Fig. 3). Six out of seven such models possess a high P_{3D} -value, while only one out of eight models with $M \geq 6$ has a high P_{3D} . The exceptions M3k4 ($M < 6$, $P_{3D} = 5.99$ %) and M6k2a ($M \geq 6$, $P_{3D} = 46.5$ %), as well as the fact that similar gt-models (e.g. M6k2a/b/c) result in very different P_{3D} -values are, however, understandable since protostellar collapse is, in essence, a rather localised process, connected to the turbulent cloud environment only via the available mass and angular momentum inflow rate. It indicates that star formation is a highly stochastic process, influenced more strongly by local properties than by the global initial conditions, a fact which is also found, for example, by Bate et al. (2003).

The range of Mach numbers found as best explanation for the data reflects the composition of the observational sample. It mainly contains sources from Perseus, Orion, and Serpens (Froebrich (2005)). There typical Mach numbers are in the range $1 \leq M \leq 6$ (e.g. Castets & Langer (1995), Schmeja et al. (2005)). It is, however, interesting to note that the majority of gt-models with $M \geq 6$ are not able to explain the observations, independent of the choice for the e-model parameters. This indicates that the ini-

tial conditions do influence the observational properties of Class 0 protostars.

3.6 Underluminous sources

We recall that we excluded 25 % of the observational data in our determination of P_{3D} . Those excluded exhibit a much lower bolometric luminosity than the other objects, for their given bolometric temperature and envelope mass. They could be objects which experience either (a) quiescent states of low accretion or (b) a different time dependence of the accretion rate (Froebrich (2005)).

A detailed investigation of the individual accretion rates from the gt-models rules out the existence of quiet accretion phases as the dominant cause for the low luminosity of these sources. On average, the individual model stars spend less than 5 % of their time in a phase of suppressed accretion which we define as being a factor of six lower than the average value. This implies that we should observe only about 5 % of the sources in such a state, compared to 25 %. Hence, these objects appear to follow a different accretion history.

We investigate this in more detail by performing the procedure of determining P_{3D} using not only the ‘normal’ sources, but also the Taurus-like objects. We find that this reveals worse agreement with P_{3D} values typically halved. The agreement between models and observations is always lower when we try to explain the Taurus like sources. This strengthens the proposal that in the case of ‘normal’ sources, turbulence governs the accretion process, while other processes are responsible for the underluminous objects. Considering their lower luminosity and hence lower accretion rates, we speculate that ambipolar diffusion might be an important process governing accretion in these sources.

A more detailed analysis of a sub-sample of Taurus like objects would be desirable since the time dependence of the mass accretion rate might vary from region to region (Henriksen et al. (1997)). Even though more and more such objects are discovered (e.g. Young et al. (2004)), indicating that the known percentage of these objects is clearly a lower limit, the current sample still suffers from too small number statistics to perform a reliable statistical analysis.

3.7 Further discussion

As evident from Table 2, the best agreement between observations and models is rather low (≈ 70 %). Here we will discuss three possible causes for this:

1. Our procedure: There are many free parameters which, in principle, could take values within a large range, as noted in Table 1. A straightforward test of all possible combinations to solve this highly non-linear minimisation problem of many variables is impossible. We thus applied a Monte Carlo method to obtain the best fitting parameter combination (see Appendix C). The obtained probability P_{3D} is a lower limit since not all possible parameter combinations have been tested. Note that only slightly smaller values for D_{3D} can lead to probabilities much closer to 100 %, especially for models that already possess a high agreement.

When converting D_{3D} to P_{3D} we restricted the random selection to model values with bolometric temperatures smaller than 80 K. This is the limit of our observational sample of Class 0 sources. There are further restrictions in the observational data. No objects outside a given range in L_{bol} and M_{env} . This is most likely an observational bias. We refrain from applying the other observational

limits for the random selection process for the P_{3D} determination because the observational limits are not well defined/understood. If doing so, however, we would increase the probabilities for the agreement in many cases significantly towards 100 %.

2. Observational data: As stated above, the observations clearly cover only a limited range of the T_{bol} - L_{bol} - M_{env} parameter space. All limits, except $T_{bol} < 80$ K, are observational biases. Note that the observational sample consists of sources from several star forming regions. It is possible that e.g. the sensitivity limit for the bolometric luminosity is not the same in all regions, changing the observed statistics of low luminosity/mass sources compared to the real one.

As shown in Fig. 1, applying a fixed limit for T_{bol} as a divide between Class 0 and Class 1 objects is not valid (see also Young & Evans (2005)). Most of the solar mass stars undergo this transition at temperatures close to 80 K. However, depending on the individual accretion history of each star, some quite significant deviations from this value are evident. Furthermore, lower mass Class 0/Class 1 transition objects tend to be warmer than the temperature limit applied here. Thus, the object sample might suffer from misclassified objects. This also shows that there is a difference in the definition for Class 0 protostars based on observations and models. Furthermore, the observational definition describes a different physical state of the object depending on its accretion history and final mass. We overcome most of these uncertainties, however, by applying the $T_{bol} < 80$ K restriction when determining P_{3D} .

3. The models: All our models are constructed on the most basic principles (e.g. the gt-models neglect feedback mechanisms, the disc mass is a constant fraction of the envelope mass, etc.). In addition, all model stars are treated with the same set of e-model parameters. It is not clear if some of the parameters might depend on the final mass of the star. Many parameters are also kept constant in time. This might not be valid (e.g. the inner envelope radius, the fraction of mass in the disc, and the powerlaw index of the envelope density distribution could depend on the evolutionary state, final mass of the star). It is in many cases, however, uncertain how these dependencies can be parameterised. We thus kept these parameters constant so as not to introduce even more free arbitrary parameters.

Given these three points, we conclude that a very good agreement between the models and observations should not be expected. It would rather be very worrying if our method would result in a 99 % agreement between models and observations. We further have to consider the possibility that star formation, and in particular the mass accretion process, might take such a diversity of paths that no simple unifying model can expect to capture them all, leading to low agreements even for future much improved observational samples and models.

4 CONCLUSIONS

We extracted mass accretion rates within cores generated by gravoturbulent simulations and inserted them into a simple protostellar evolutionary scheme to calculate protostellar evolutionary tracks. A principle dependence of the position of these tracks in the T_{bol} - L_{bol} diagram on the final mass is found. A detailed analysis, however, shows that we are not able to determine the final mass of a particular object from its measured bolometric temperature and luminosity more accurately than a factor of two. The particular shape of an evolutionary track is largely determined by the accretion history and by its final mass. Hence, in the context of the gravoturbulent

scheme, unique evolutionary tracks do not exist in the Class 0 or Class 0/1 phase, as opposed to the ensuing pre-main sequence evolution. It also implies that T_{bol} is not always a reliable guide to the envelope-protostar mass ratio, as suggested also by Young & Evans (2005).

A 3D-KS-test was used to compare the distribution of our evolutionary tracks in the T_{bol} - L_{bol} - M_{env} parameter space with an observational sample of Class 0 objects. By varying free parameters associated with the evolutionary scheme, we are able to determine constraints for some of the parameters (T_{env} , $frac_{env}$, M_{extra} , M_{eff} , p). Others were found to have no significant influence on the agreement between models and observations (t_0 , α , R_{in} , κ). A comparison of the parameter values obtained by our method with observational constraints from individual objects (e.g. for $frac_{env}$ or p) can be conducted. This supports the reliability of our method as similar parameter values are obtained.

Only gravoturbulent models generating model stars with a specific density at the start of the collapse and Class 0 lifetimes between 2 and $6 \cdot 10^4$ yrs lead to a good agreement with the observations. This Class 0 lifetime is consistent with estimates of a few 10^4 yrs based on number ratios or dynamical timescales of outflows (see e.g. André et al. (2000)). It is shown that the Class 0 lifetime is correlated with the local density at the onset of the collapse. The determined density range agrees well with density measurements for pre-stellar cores.

Gravoturbulent models with $0.5 \leq M \leq 3$ lead to the best agreement with the observations. The failure of models with $M \geq 6$ to explain the data indicates that the initial conditions influence the observational properties of Class 0 sources. The initial mass function appears not to influence the agreement systematically. The highest probability that our distributions of model tracks and observational data points are drawn from the same basic population is 70 %. This is reasonable given the uncertainties in the observations and the simple assumptions in the models. However, the method can be readily adapted to compare larger future source samples, different sets of accretion rates or other envelope models.

Applying the KS-test to both the ‘normal’ and underluminous, ‘Taurus-like’ objects in the source sample, we find that the determined probability P_{3D} is about twice as large when testing the ‘normal’ objects. This is consistent with the proposal that turbulence governs the accretion rates in the majority of the objects.

ACKNOWLEDGEMENTS

We thank A. Scholz for tirelessly answering questions about the 3D-KS method. D. Froebrich received financial support from the Cosmo-Grid project, funded by the Program for Research in Third Level Institutions under the National Development Plan and with assistance from the European Regional Development Fund. S. Schmeja and R.S. Klessen acknowledge support by the Emmy Noether Programme of the Deutsche Forschungsgemeinschaft (grant no. KL1358/1). Research at Armagh Observatory is funded by the Department of Culture, Arts and Leisure, Northern Ireland.

REFERENCES

- Adams, F.C., Lada, C.J., & Shu, F.H. 1987, ApJ, 312, 788
 André, P., Ward-Thompson, D., & Barsony, M. 1993, ApJ, 406, 122

André, P., Ward-Thompson, D., & Barsony, M. 2000, in *Protostars and Planets IV*, 59

Bacmann, A., Lefloch, B., Ceccarelli, C., Castets, A., Steinacker, J. & Loinard, L. 2002, *A&A*, 389, L6

Bate, M.R., & Burkert, A. 1997, *MNRAS*, 288, 1060

Bate, M.R., Bonnell, I.A., & Bromm, V. 2003, *MNRAS*, 339, 577

Bate, M.R., Bonnell, I.A., & Price, N.M. 1995, *MNRAS*, 277, 362

Bontemps, S., André, P., & Ward-Thompson, D. 1995, *A&A*, 297, 98

Bontemps, S., André, P., Terebey, S., & Cabrit, S. 1996, *A&A*, 311, 858

Bourke, T.L., Garay, G., Lehtinen, K.K., et al. 1997, *ApJ*, 476, 781

Castets, A. & Langer, W.D. 1995, *A&A*, 294, 835

Chandler, C.J. & Richer, J.S. 2000, *ApJ*, 530, 851

Chen, H., Myers, P.C., Ladd, E.F., & Wood, D.O.S. 1995, *ApJ*, 445, 377

Davis, C.J., Smith, M.D., & Moriarty-Schieven, G.H. 1998, *MNRAS*, 299, 825

Foster, P.N. & Chevalier, R.A. 1993, *ApJ*, 416, 303

Froebrich, D. 2005, *ApJS*, 156, 169

Froebrich, D., Smith, M.D., Hodapp, K.-W., & Eislöffel, J. 2003, *MNRAS*, 346, 163

Henriksen, R., André, P., Bontemps, S. 1997, *A&A*, 323, 549

Hurt, R.L., & Barsony, M. 1996, *ApJ*, 460, 45

Jappsen, A.-K., & Klessen, R.S. 2004, *A&A*, 423, 1

Kenyon, S.J., Hartmann, L.W., Strom, K.M. & Strom, S.E. 1990, *AJ*, 99, 869

Klessen, R.S. 1997, *MNRAS*, 292, 11

Klessen, R.S. 2001a, *ApJ*, 550, 77

Klessen, R.S. 2001b, *ApJ*, 556, 837

Klessen, R.S., Heitsch, F., & Mac Low, M.-M. 2000, *ApJ*, 535, 887

Larson, R.B. 1969, *MNRAS*, 145, 271

Larson, R.B. 2003, *Rep. Prog. Phys.*, 66, 1651

Laughlin, G., & Różyczka, M. 1996, *ApJ*, 456, 279

Looney, L.W., Mundy, L.G., Welch, W.J. 2003, *ApJ*, 592, 255

Mac Low, M.-M., & Klessen, R.S. 2004, *Rev. Mod. Phys.*, 76, 125

Monaghan, J.J. 1992, *ARA&A*, 30, 543

Motte, F., & André, P. 2001, *A&A*, 365, 440

Myers, P.C., Adams, F.C., Chen, H., & Schaff, E. 1998, *ApJ*, 492, 703

O'Linger, J., Wolf-Chase, G., Barsony, M., & Ward-Thompson, D. 1999, *ApJ*, 515, 696

Padman, R., Bence, S., & Richer, J. 1997, in 'Herbig-Haro Flows and the Birth of Stars' *IAUS 182*, Ed. B Reipurth & C. Bertout, Kluwer Academic Publishers, 123

Padoan, P., & Nordlund, Å. 2002, *ApJ*, 576, 870

Papaloizou, J.C.B., & Lin, D.N.C. 1995, *ARA&A*, 33, 505

Penston, M.V. 1969, *MNRAS*, 145, 457

Pringle, J.E. 1981, *ARA&A*, 19, 137

Salpeter, E.E. 1955, *ApJ*, 121, 161

Saraceno, P., André, P., Ceccarelli, C., Griffin, M., & Molinari, S. 1996, *A&A*, 309, 827

Schmeja, S., & Klessen, R.S. 2004, *A&A*, 419, 405

Schmeja, S., Klessen, R.S., & Froebrich D. 2005, *A&A*, 437, 911

Shirley, Y.L., Evans II, N.J., Rawlings, J.M.C., & Gregersen, E.M. 2000, *ApJS*, 131, 249

Shu, F.H. 1977, *ApJ*, 214, 488

Shu, F.H., Li, Z.-Y., & Allen, A. 2004, *ApJ*, 601, 930

Singh, S., Ma, C.-P., & Arons, J. 2004, *Phys. Rev. D*, 69, 3003

Smith M.D. 1998, *Ap&SS*, 261, 169

Smith, M.D. 2000, *IrAJ*, 27, 25

Smith, M.D. 2002, In: *The Origins of Stars and Planets: The VLT View*, João Alves & Mark McCaughrean (ed.), CD-ROM.

Stanke, T. 2000, Ph.D. thesis (AIP, Potsdam)

Stanke, T., McCaughrean, M.J., & Zinnecker, H. 2002, *A&A*, 392, 239

Tomisaka, K. 1996, *PASJ*, 48, 97

Whitworth, A.P., & Ward-Thompson, D. 2001, *ApJ*, 547, 317

Wuchterl, G., & Klessen, R.S. 2001, *ApJ*, 560, 185

Wuchterl, G., & Tscharnuter, W.M. 2003, *A&A*, 398, 1081

Young, C.H. & Evans II, N.J. 2005, *ApJ*, 627, 293

Young, C.H., Jørgensen, J.K., Shirley, Y.L., et al. *ApJS*, 154, 396

Yu, K.C., Billawala, Y., Smith, M.D., Bally, J., & Butner, H.M. 2000, *AJ*, 120, 1974

Ziener, R., & Eislöffel, J. 1999, *A&A*, 347, 565

APPENDIX A: GRAVOTURBULENT MODELS

Our simulations describe the evolution of (1) two globally unstable model clouds that contract from Gaussian initial conditions without turbulence and (2) 22 models where turbulence is maintained with constant root mean square Mach numbers. The models are labelled G1/G2 for the Gaussian, and M/Mk (with rms Mach number M and wavenumber k) for the turbulent models, following SK04. The designators a, b, c distinguish models that have the same M and k values, but different random realisations of the turbulent driving field; they also differ in the time when self-gravity is 'switched on'.

The gt-models are computed in normalised units. To scale to physical units, we adopt a mean density of $n(\text{H}_2) = 10^5 \text{ cm}^{-3}$ and a temperature of 11.3 K corresponding to a sound speed $c_s = 0.2 \text{ km s}^{-1}$. For the two Gaussian models, the total mass present is $220 M_\odot$ and the size of the cube is 0.34 pc. For the turbulent models, the cube contains a mass of $120 M_\odot$ within a volume of $(0.28 \text{ pc})^3$. The mean thermal Jeans mass in all models is $\langle M_J \rangle = 1 M_\odot$ and the global free-fall timescale is $\tau_{\text{ff}} = 10^5 \text{ yr}$. Requiring that the local Jeans mass is always resolved by at least 100 gas particles (Bate & Burkert (1997)), the resolution limit is $0.058 M_\odot$ in all our turbulent models and $0.044 M_\odot$ in the Gaussian models.

The radius of a sink particle is fixed at 280 AU. Infalling gas particles undergo several tests to check if they remain bound to the sink particle before they are considered accreted. We cannot resolve the evolution in the interior of the control volume defined by the sink particle. Because of angular momentum conservation most of the infalling matter will accumulate in a protostellar disc within which it is transported inwards by viscous and possibly gravitational torques (Pringle (1981); Papaloizou & Lin (1995); see also Jappsen & Klessen (2004) for the models discussed here). The latter will be provided by spiral density waves that develop when the disc becomes too massive. This occurs when mass is loaded onto the disc faster than it is removed by viscous transport. Altogether, the disc will not prevent or delay material from accreting onto the protostar for long. It acts as a buffer and smoothes possible accretion spikes. For the mass range considered here feedback effects are too weak to halt or delay accretion (Wuchterl & Klessen (2001); Wuchterl & Tscharnuter (2003)). With typical disc sizes of the order of a few hundred AU, the control volume encloses both protostar and disc. The measured core accretion rates are hence good estimates of the actual stellar accretion rates. Strong deviations may be expected only if the protostellar core fragments into a binary system, in which case the infalling mass is distributed over two stars.

In addition, if material with very high angular momentum is accreted, a certain mass fraction may end up in a circumbinary disc and not accrete onto the star at all.

The timescale over which accretion is smoothed by the disc can be approximated by the viscous timescale

$$t_v \approx \alpha_v^{-1} (R/H)^2 t_\phi \quad (\text{A1})$$

(Pringle (1981)), with the viscosity parameter α_v , the disc radius R , the disc scale height H , and the rotational period $t_\phi = \Omega^{-1}$. Using typical values of $\alpha_v = 0.01$, $R/H = 10$ and $t_\phi = 1$ yr this yields a rough estimate of $t_v \approx 10^4$ yrs for the viscous timescale at a radius of 1 AU. A large fraction of mass will lie external to this radius, leading to a larger t_v , but this will be compensated for by stronger gravitational torques, which can lead to significantly larger values of the effective viscosity in the disc (see e.g. Laughlin & Różyczka (1996)). Since we cannot model the detailed behaviour inside the disc, we take 10^4 yrs as a rough measure for the smoothing timescale. This value is used to smooth the individual mass accretion rates from the gt-models. Our results do not significantly depend on the smoothing scale that we apply. Adopting viscous timescales of 5 or $15 \cdot 10^3$ yrs yields very similar results.

There are further smoothing effects and time-shifts, e.g. the luminosity generated in the centre typically escapes a Class 0 envelope in about 300 yrs (as determined by a random walk model). Hence, this time lag is neglected in comparison to the disc viscosity timescale. The viscosity of the disc has additionally the effect that material transported from the envelope onto the disc needs some time before it gets accreted onto the star and the accretion luminosity is generated. Hence, the observed envelope masses and luminosities do not represent the same time in the evolution. The observed luminosity corresponds to that of an envelope mass which was present about a viscosity timescale earlier. However, since this effect does not become significant until the disc is formed, it can be neglected in the very early stages of the evolution. In later stages, the evolution along the $T_{\text{bol}}\text{-}L_{\text{bol}}$ track is slower and the luminosity only slightly changes within one viscosity timescale. In particular the change is smaller than typical errors of the measurements. Hence, we also neglect this effect in our calculations.

APPENDIX B: EVOLUTIONARY MODEL

Accretion rates applied in the e-model to date assume specific functional forms with a fixed time scale for all protostars. As a consequence, even without a statistical comparison, it fails to explain the data. To overcome this, new parameters were introduced by Myers et al. (1998). They took different evolutionary timescales for the envelope and the accretion, and subsequently found that the observations required (1) the accretion time scale to exceed the envelope timescale by a factor of a few and (2) the final mass of the star to be quite a small fraction of the original envelope mass.

In addition, there are several free parameters in the e-model. Some of their values are not as yet tightly constrained through observations or theory. Plausible values, however, predict evolutionary tracks across the same region as occupied by the observed protostars (e.g. Froebrich et al. (2003)). Nevertheless, an immediate problem encountered with the basic model was that the protostars spent little time in the early Class 0 phase but lingered in the late Class 0 phase for periods exceeding 10^5 yr, implying contrary statistics to those observed. To overcome this, a distinct mass component was introduced into the envelope. In the e-model, this arbitrary mass would not accrete, but would be dispersed directly. The

rationale was that star formation remains inefficient due to outflow activity from the protostar. The second arbitrary parameter was the fraction of mass contained within a flattened distribution. That is, it is assumed from the outset, that a small fraction of the gas is available to accrete but does not add to the obscuration of the protostar. However, given these additions, it becomes difficult to relate the predictions uniquely to the chosen parameter set through the KS-test if we attempt to calculate analytically which parameter values would lead to the highest agreement between models and observations.

Additional free parameters in the e-model are an inner density, and inner and outer radius for the envelope. We have generalised the previous studies by introducing a power-law index (p) for the radial density distribution, where $\log \rho \propto -p \times \log R$, rather than fixing the value at 1.5. Instead of the inner density we employ the total envelope mass as the variable. In addition, rather than the outer radius, we adopt the outer temperature T_{env} as the variable which then determines the outer radius. Most of the mass initially contained in the envelope will eventually fall onto the protostar. The accretion luminosity depends on the collapse radius and the contraction of the central hydrostatic object. Here, we assume that a constant density core develops.

Equations

In the following we describe in more detail the equations and parameters used in the evolutionary model for this work.

The initial mass of the envelope and circumstellar disk, M_0 , is found by integrating the mass accretion rate, $\dot{M}_a(t)$, over time. Hence, the envelope/disk mass is given by

$$M_{\text{e,d}}(t) = M_0 - \int_0^t \dot{M}_a(t') \cdot dt'. \quad (\text{B1})$$

The mass just in the spherical envelope is taken as

$$M_{\text{env}}(t) = \text{frac}_{\text{env}} \cdot M_{\text{e,d}}(t). \quad (\text{B2})$$

In the first approximation, the accreting material is taken as instantaneously reaching the central hydrostatic core, defining the protostellar radius, R_* . A fraction $(1 - \eta(t))$ of this material is accreted onto the star i.e.

$$M_*(t) = \int_0^t (1 - \eta(t')) \cdot \dot{M}_a(t') \cdot dt'. \quad (\text{B3})$$

The parameter $\eta(t)$ will depend on the jet launching mechanism. We suppose that it is a function of the relative accretion rate i.e.

$$\eta(t) = M_{\text{eff}} \cdot \left[\frac{\dot{M}_a(t)}{\dot{M}_{\text{max}}} \right]^\zeta \quad (\text{B4})$$

where \dot{M}_{max} is the peak accretion rate and $\zeta = 2$ has been assumed to date. Thus, M_{eff} is the maximum fraction of material ejected into the jets.

We assume here that the hydrostatic core grows at constant density during the very early stages of star formation (no energy released through contraction):

$$\frac{R_*(t)}{R_\odot} = 4.24 \cdot \left[\frac{M_*(t)}{M_\odot} \right]^{1/3} \cdot \left[\frac{M_0}{M_\odot} \right]^{2/3}. \quad (\text{B5})$$

We have found that alternative treatments produce similar results. The particular dependence on envelope mass corresponds to the case where the final escape speed of the jets is constant.

The gravitational energy released is assumed to end up in radiation or in the jets. We thus write the accretion luminosity as

$$L_{\text{acc}}(t) = (1 - \eta(t)) \cdot G \cdot \dot{M}_a(t) \cdot M_*(t)/R_*(t). \quad (\text{B6})$$

The initial *cloud core* mass could exceed the *envelope* mass. That is, some extra mass is introduced. This mass is dispersed rather than being accreted. In other words, we can check to see if there is some form of feedback or turbulent dissipation in operation which maintains a cooler core during the early stages. We assume a form

$$M_{\text{core}}(t) = M_{\text{env}}(t) \cdot \left[1 + M_{\text{extra}} \cdot \left(\frac{t + t_0}{t_0} \right)^{-2\alpha} \right], \quad (\text{B7})$$

where α and t_0 describe the dissipation of M_{extra} . Note that for $M_{\text{extra}} = 0$ the particular values for t_0 and α are superfluous and $M_{\text{core}}(t)$ is equal to $M_{\text{env}}(t)$.

The radius corresponding to the outer edge of the envelope is determined by an assumed outer temperature, T_{env} :

$$R_{\text{env}}(t) = \frac{1}{T_{\text{env}}^2} \cdot \left[\frac{L_{\text{acc}}(t)}{2\pi \cdot \sigma} \right]^{1/2}, \quad (\text{B8})$$

where σ is the Stefan-Boltzmann constant.

Given an inner radius for the envelope, R_{in} (possibly fixed by the centrifugal barrier condition) and a power-law radial distribution of density with index $-p$, the inner density of the envelope can be written

$$\rho_{\text{in}}(t) = \frac{(3 - p) \cdot M_{\text{core}}(t)}{4\pi \cdot R_{\text{in}}^3 \cdot \varepsilon(t)} \quad (\text{B9})$$

where

$$\varepsilon(t) = \left(\frac{R_{\text{env}}(t)}{R_{\text{in}}} \right)^{3-p} - 1. \quad (\text{B10})$$

The inner temperature of the envelope is

$$T_{\text{in}}(t) = \left[\frac{L_{\text{acc}}(t)}{2\pi \cdot \sigma \cdot R_{\text{in}}^2} \right]^{1/4}. \quad (\text{B11})$$

This yields an optical depth through the envelope proportional to the emissivity:

$$\tau_e(t) = \kappa \cdot \rho_{\text{in}}(t) \cdot R_{\text{in}} \cdot \frac{1 - \varepsilon(t)^{1-p}}{p - 1}. \quad (\text{B12})$$

Following Myers et al. (1998), we take κ as the emissivity at $12 \mu\text{m}$, $A = 1.59 \cdot 10^{-13} \text{ cm}^2 \text{ g}^{-1} \text{ Hz}^{-1}$, h as the Planck constant, k the Boltzmann constant, and calculate the bolometric temperature:

$$T_{\text{bol}}(t) = \frac{\Gamma(9/2) \cdot \zeta(9/2)}{\Gamma(5) \cdot \zeta(5)} \cdot \left[\frac{h \cdot \kappa \cdot T_{\text{in}}(t)}{k \cdot A \cdot \tau_e(t)} \right]^{1/2}. \quad (\text{B13})$$

APPENDIX C: 3D KS-TEST AND PROBABILITIES

To evaluate how well observations and models match, we need to determine the KS-parameter $D_{3\text{D}}$. First, we note that each data point (T_{bol}^i , L_{bol}^i , M_{env}^i) can be used to dissect the parameter space into eight octants. The difference D_i between the fraction of model data points and observational data points in each of the eight octants in the $T_{\text{bol}}\text{-}L_{\text{bol}}\text{-}M_{\text{env}}$ parameter space is calculated for each data point. Here, the index i covers *both the observational and model data* points. In case of N data points, this procedure results in $8N$ numbers D_i . The maximum absolute difference value is then defined as the KS-parameter $D_{3\text{D}} = \text{MAX}(|D_i|)$. Note that this value can range from zero to one.

As described in Sect. 2.1 and 2.2, the restrictions in the source sample and models lead to the problem that we have to compare two samples with extremely different sizes. The observational sample consists of 27 points. Depending on the set of accretion rates we use, the model sample consists of about ten thousand points (100 tracks of individual stars and on average 100 points per single track, considering our timestep of 300 yrs and assuming a lifetime of $3 \cdot 10^4$ yrs for Class 0 sources). Hence, the test described above has to be performed about 10^4 times to determine $D_{3\text{D}}$ for one case, resulting in a huge amount of computations. Since we are only interested in the maximum of the absolute differences between the relative numbers of the model points and observational points in the octants, we can constrain the investigated area to a cuboid containing all the observational data-points. A test outside these boundaries will not lead to absolute differences larger than obtained inside the cuboid. In other words, $\text{MAX}(|D_i|)$ corresponds to a point situated inside or at the boundary of the cuboid defined as: $[T_{\text{bol}}^{\text{obs,min}} < T_{\text{bol}} < T_{\text{bol}}^{\text{obs,max}}; L_{\text{bol}}^{\text{obs,min}} < L_{\text{bol}} < L_{\text{bol}}^{\text{obs,max}}; M_{\text{env}}^{\text{obs,min}} < M_{\text{env}} < M_{\text{env}}^{\text{obs,max}}]$. However, since most of the model points are still situated within this cuboid, the required amount of computations is not significantly reduced.

Hence, we do not perform the test at all data points within this area, but rather at a certain number of points inside the cuboid. We performed extensive tests in order to establish the best compromise between computing time (number of points where the test has to be performed) and the accuracy of the method. As a result, we found that a $5 \times 5 \times 5$ point grid in the cuboid is sufficient to determine $D_{3\text{D}}$ with the same accuracy as the probability of the agreement between observations and models (see below). The ranges in T_{bol} , L_{bol} , and M_{env} are thus divided into four equally sized regions. While for T_{bol} linear spacing was chosen, L_{bol} and M_{env} are divided into equal spaces in logarithmic units.

In order to convert the $D_{3\text{D}}$ value into a probability of agreement $P_{3\text{D}}$, a Monte Carlo method has to be applied. For this purpose, we generated artificial observational data points by randomly selecting 27 model points out of all model points and treating them as observational data. Since the observational data is limited to $T_{\text{bol}} < 80 \text{ K}$, we applied this limit for the random selections as well. Then the KS-test was performed (using the same grid positions as with the real observational data points), leading to a value $D_{3\text{D}}^{\text{MC}}$. Repeating this process, a distribution $N(D_{3\text{D}}^{\text{MC}})$ is created. The probability $P_{3\text{D}}$ can then be determined by:

$$P_{3\text{D}} = \int_{D_{3\text{D}}}^1 N(D_{3\text{D}}^{\text{MC}}) \Big/ \int_0^1 N(D_{3\text{D}}^{\text{MC}}) \quad (\text{C1})$$

All $D_{3\text{D}}$ -values need to be converted to $P_{3\text{D}}$ by such a Monte Carlo simulation. To minimise the computational needs we tested if this is needed for every single $D_{3\text{D}}$ -value. It turned out that the distributions $N(D_{3\text{D}}^{\text{MC}})$ obtained by a Monte Carlo simulation for one gt-model but different parameter sets in the e-model are similar. Hence all $D_{3\text{D}}$ -values of one gt-model can be converted into $P_{3\text{D}}$ using the same distribution. However, distributions $N(D_{3\text{D}}^{\text{MC}})$ for distinct gt-models are partly very different. Thus, to find the best fitting model combination we selected the parameter combination leading to the smallest $D_{3\text{D}}$ -value for each gt-model to determine $N(D_{3\text{D}}^{\text{MC}})$. This was then used to calculate the agreement $P_{3\text{D}}$.

The total number of random selections to build up the distribution $N(D_{3\text{D}}^{\text{MC}})$ was a critical point concerning the accuracy of the method. Hence, we tested for which number of repeats the final values of $P_{3\text{D}}$ did not vary by more than one percent if the same test was repeated. For our distribution of model points, this was the

case for $3 \cdot 10^4$ random selection processes. This accuracy is not degraded by the $5 \times 5 \times 5$ grid, chosen for performing the KS-test, instead of doing the test at all datapoints in the cuboid.

There are nine free parameters in the e-models which we kept variable. Our task here is to find the combination of these parameters that leads to the best agreement with the models. A test of all possible combinations with an accurate spacing requires an immense amount of computations. We thus decided to use a Monte Carlo approach for this task as well. We randomly selected 100 values for each parameter from the range given in Table 1 and determined D_{3D} for these 100 random combinations. We then selected the parameter sets that lead to D_{3D} -values which were smaller than $(D_{3D}^{\max} + D_{3D}^{\min})/2$. The maximum and minimum for each parameter value used in these selected sets was then taken to re-set the ranges out of which parameter values are selected. Then again 100 e-models with randomly selected parameters out of the new range were tested. This procedure was repeated 30 times, finally leading to 3100 tested e-models. These models are used to determine the best fitting parameter ranges (Table 2) for the individual gt-models. These ranges were then used to determine another 10000 random parameter combinations, in order to find the best agreement.

We tested for a subset of parameters and smaller ranges if the Monte Carlo method leads to the same results as a straight forward testing of all possible parameter combinations. Both, the smallest D_{3D} -value and the best fitting ranges for the parameter values, are found to be similar. Note that the smallest found D_{3D} -value has to be considered an upper limit, since not the whole parameter space was tested. Alternatively the probability P_{3D} is a lower limit.